Possible large near-trench slip during the 2011 M_w 9.0 off the Pacific coast of Tohoku Earthquake

Thorne Lay[1], Charles J. Ammon[2], Hiroo Kanamori[3], Lian Xue[1], and Marina J. Kim[1]

[1]*University of California Santa Cruz, Santa Cruz, California 95064, USA*
[2]*The Pennsylvania State University, University Park, Pennsylvania 16802, USA*
[3]*California Institute of Technology, Pasadena, California 91125, USA*

(Received April 7, 2011; Revised May 22, 2011; Accepted May 25, 2011; Online published September 27, 2011)

The 11 March 2011 off the Pacific coast of Tohoku (M_w 9.0) Earthquake ruptured a 200 km wide megathrust fault, with average displacements of ∼15–20 m. Early estimates of the co-seismic slip distribution using seismic, geodetic and tsunami observations vary significantly in the placement of slip, particularly in the vicinity of the trench. All methods have difficulty resolving the up-dip extent of rupture; onshore geodetic inversions have limited sensitivity to slip far offshore, seismic inversions have instabilities in seismic moment estimation as subfault segments get very shallow, and tsunami inversions average over the total region of ocean bottom uplift. Seismic wave estimates depend strongly on the velocity structure used in the model, which affects both seismic moment estimation and inferred mapping to slip. We explore these ideas using a least-squares inversion of teleseismic P-waves that yields surprisingly large fault displacements (up to ∼60 m) at shallow depth under a protrusion of the upper plate into the trench. This model provides good prediction of GPS static displacements on Honshu. We emphasize the importance of poorly-constrained rigidity variations with depth for estimating fault displacement near the trench. The possibility of large slip at very shallow depth holds implications for up-dip strain accumulation and tsunamigenic earthquake potential of megathrusts elsewhere.

Key words: 2011 Tohoku Earthquake, megathrust faults, subduction zones, earthquake rupture process, tsunami earthquakes.

1. Introduction

It is challenging to constrain the up-dip limit of great earthquake ruptures such as the 11 March 2011 Tohoku (M_w 9.0) event. The geophysical signals available to address this problem include seismic and geodetic ground motion recordings, tsunami recordings, aftershock distributions, and in some cases, bathymetric pressure sensors and imaging of coseismic changes in the seafloor. All of these methods have limitations when they are used to image up-dip fault motion in the presence of large deeper fault motions along the megathrust. However, the problem is important; establishing whether or not the up-dip region has failed in a great earthquake is central to assessing the potential for future earthquakes that can be particularly tsunamigenic. The 1907 Sumatra (Kanamori *et al.*, 2010) and 2010 Mentawai (M_w 7.8) (Lay *et al.*, 2011a) tsunami earthquakes ruptured narrow margins up-dip of deeper great underthrusting ruptures, and produced larger tsunami run-ups than did the larger, but deeper events adjacent to them. The occurrence of tsunami earthquakes, which characteristically have long source process times and weak short-period radiation (e.g., Kanamori, 1972; Kanamori and Kikuchi, 1993; Polet and Kanamori, 2000; Bilek and Lay, 2002; Ammon *et al.*, 2006) must involve rather large ocean bottom deformations indicative of large slips on the megathrust or on splay faults (Fukao, 1979; Pelayo and Wiens, 1992). The up-dip limit of co-seismic slip in large earthquakes is also important for consideration of how stresses are communicated to the trench-slope and outer rise intraplate environments, and the potential for tsunamigenic normal faulting ruptures (Kanamori, 1971; Ammon *et al.*, 2008; Lay *et al.*, 2011c). Given the common presence of a sedimentary wedge and the relatively hydrated conditions likely to exist in a shallow megathrust, it is usually uncertain whether the frictional regime will favor stable sliding or large strain accumulation.

The 11 March 2011 Tohoku Earthquake ruptured a wide (∼200 km) region of the megathrust, appearing to extend from near the trench to near the Honshu coastline. Preliminary models for the slip distribution of the rupture have significant differences; short-period seismic wave back-projections indicate concentration of short-period radiation from down-dip (Koper *et al.*, 2011), geodetic inversions indicate slip further off-shore, but with a significant drop-off in slip toward the trench (e.g., Simons *et al.*, 2011), and broadband seismic wave inversions indicate primary seismic moment contributions from up-dip of the hypocenter, possibly extending to the trench (e.g., Ammon *et al.*, 2011). Some of these differences may be reconciled by frequency-dependent variations in seismic wave radiation from the down-dip and up-dip regions (e.g., Koper *et al.*, 2011). Geodetic inversions for this event are confronted

doi:10.5047/eps.2011.05.033

with the challenge of poor azimuthal coverage of the source region and the possibility of stronger slip located further off-shore matching the data as well as lesser slip at greater depth closer to shore. Seismic inversions involve dependence on rupture expansion kinematics, near-source seismic velocity structure, and intrinsic sensitivity of various seismic phases to rupture finiteness. Tsunami observations can provide good timing constraints on the location of seafloor motions, potentially constraining slip at shallow depths, but the long wavelengths involved do require accounting for the full spatial extent of source motions (Lay *et al.*, 2011b). We explore some of these issues in the context of a seismic wave inversion solution that favors large fault displacements near the trench for the Tohoku event (Fig. 1).

2. The 11 March 2011 Rupture

Teleseismic broadband P-waves were inverted using a least-squares linear inversion procedure for a finite-fault model representation (developed by M. Kikuchi and H. Kanamori), based on the algorithm of Hartzell and Heaton (1983). The resulting model, which we label P-MOD2 is shown in Figs. 1 and 2. The fault was prescribed to have ten 20×20 km^2 subfaults along a 10° dip and 19 along a strike of 202°, spanning a total area of 76,000 km^2. Each subfault has a source time function parameterized by seven 8 s wide symmetric triangles, offset by 4 s each, yielding 32 s long subfault rupture durations. The moment and rake of each subevent triangular time function element are the unknowns in the inversion. The rupture is constrained to grow outward on the fault relative to a specified hypocenter at 1.5 km/s to a distance of 100 km and then at 2.5 km/s until it reaches the margins of the fault model. Our choices of these subfault and rupture kinematics parameters were based on many inversion runs for data sets of just P-waves as well as data sets with R_1 source time functions and high-rate GPS data (e.g., Ammon *et al.*, 2011), and these assumptions affect the details of the resulting models. All of the independent early finite fault inversions that we are aware of (e.g., Simons *et al.*, 2011; Ide *et al.*, 2011, and many papers in review) and all short-period back projection applications (e.g., Koper *et al.*, 2011) support low rupture velocities of 1.0–1.5 km/s during the first 60–80 s of this rupture, with subsequent more rapid expansion to the southwest.

A 1-D layered source region velocity structure adapted from Takahashi *et al.* (2004) was used to compute the subfault responses. As always, approximating the 3-D wedge structure with a 1-D model involves simplifications. We averaged the velocities in the vicinity of the megathrust to approximate a 1-D structure with appropriate along-dip variations in source parameters. We assume a 2-km ocean layer, a 4 km-thick upper crustal layer with P velocity, $V_p = 4.4$ km/s, S-wave velocity, $V_s = 2.51$ km/s, density, $\rho = 2000$ kg/m^3; a 10-km thick mid-crustal layer with $V_p = 6.0$ km/s, $V_s = 3.46$ km/s, $\rho = 2600$ kg/m^3; a 16-km thick deep crustal layer with $V_p = 6.7$ km/s, $V_s = 3.87$ km/s, $\rho = 2900$ kg/m^3; and a half-space with $V_p = 7.7$ km/s, $V_s = 4.5$ km/s, $\rho = 3300$ kg/m^3. Source region rigidities for each subfault centroid are determined from the values of V_s and ρ at corresponding depth. Several hypocenter locations were used to position the fault relative to the trench; the U.S. Geological Survey hypocenter (38.322°N, 142.369°E, 05:46:23 UTC, depth 24.4 km) was used to produce an initial solution (P-MOD), which is presented in preliminary analyses by Koper *et al.* (2011) and Lay *et al.* (2011b); but here we use a much more seaward hypocenter location (38.147°N, 142.915°E, depth 17 km) estimated by first-arrival relocation in a 3-D velocity model by Dapeng Zhao (personal communication, 2011). The Japan Meteorological Agency (JMA) hypocenter (38.103°N, 142.861°E, depth 23.7) was also considered, but as this location is intermediate to the other two, no results are shown for that particular hypocenter.

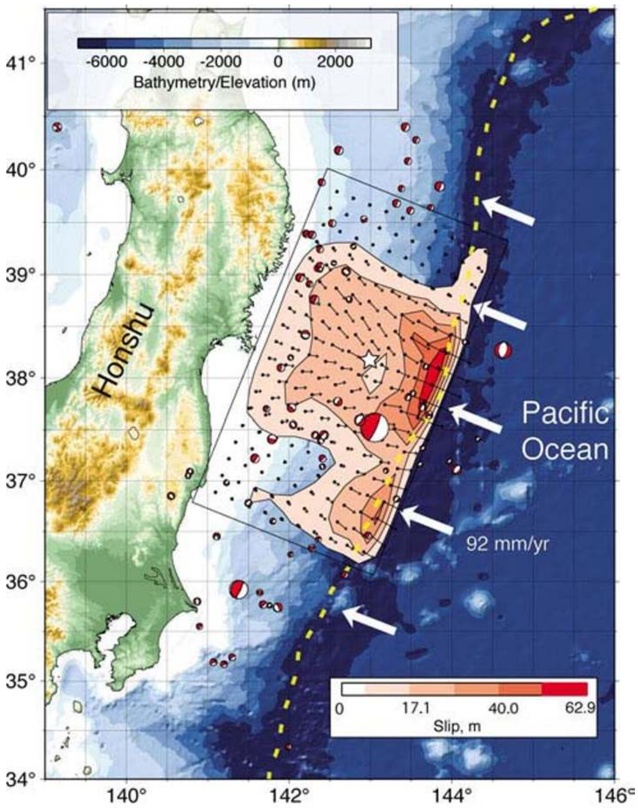

Fig. 1. Map of the 11 March 2011 Tohoku great earthquake slip model P-MOD2 obtained from least-squares inversion of teleseismic P-waves. The yellow dashed curve indicates the position of the trench deep. Focal mechanisms for the mainshock and the first 3 weeks of aftershocks from the Global Centroid Moment Tensor (GCMT) catalog are shown. White arrows indicate the MORVEL relative plate motion of the Pacific plate, holding the Japan mainland fixed.

The data set used is comprised of 38 teleseismic broadband P-wave ground motions from stations of the Federation of Digital Seismic Networks (FDSN), accessed through the Incorporated Research Institutions for Seismology (IRIS) data center. The data were selected from hundreds of available FDSN seismograms to have good azimuthal coverage and several minutes of time after the P arrival preceding the PP phase; this limits epicentral distances to be mainly greater than 50°. These data thus sample a narrow cone of take-off angles from the source (Fig. 2), and the high apparent velocities of teleseismic P-waves yield limited sensitivity to the absolute location of the features in the source. Differences in the hypocentral location cannot be resolved by the data (all three locations can produce good

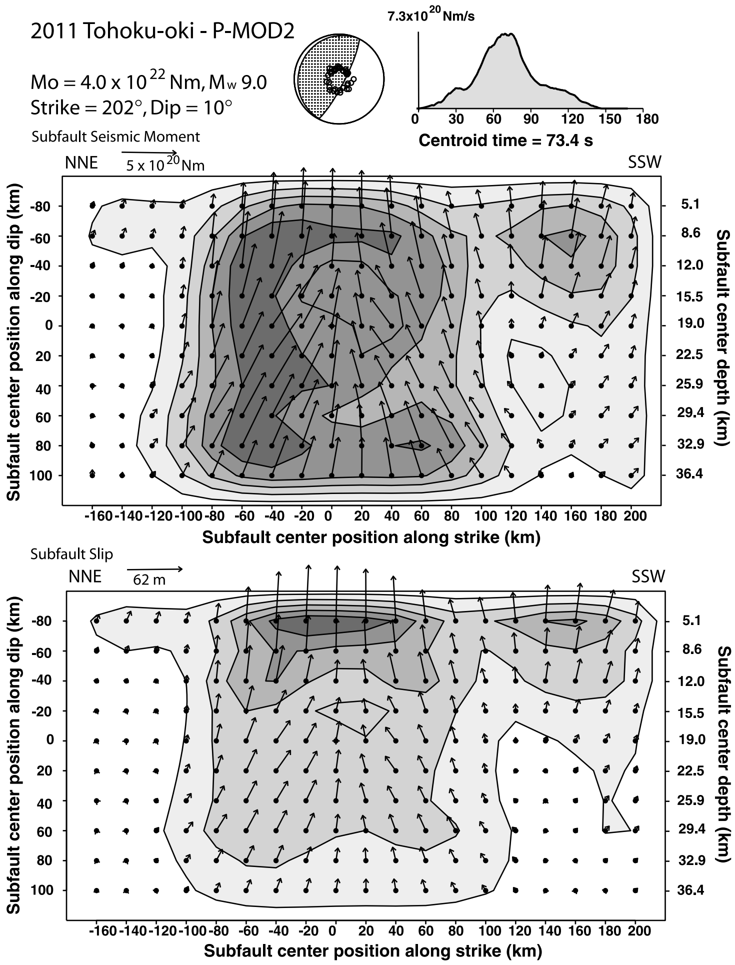

Fig. 2. P-wave inversion model P-MOD2, for the 11 March 2011 Tohoku great earthquake. This model assumed the hypocentral parameters from D. Zhao (personal communication), and allowed the model grid to extend to the furthest up-dip limit of the upper plate in the Japan trench. The focal mechanism is used to show the distribution of stations used in the inversion. The moment rate function is shown on the top right along with the centroid time. The subfault seismic moment values are indicated in the central map, with vectors indicating the average rake direction and relative moment for each subfault, and the inferred slip distribution is shown at the bottom with vectors indicating the relative slip values.

fits), but moving the location seaward initiates the rupture at shallower depth, and reduces the distance up-grid to the trench. The grid for the model here (P-MOD2) extended to a trenchward bulge of the upper plate, which causes small overlap of the rectangular source grid with the trench to the north and south. This geometric compromise allows us to explore slip estimation all the way to the trench.

The waveform fits to the teleseismic P wave ground displacements are very good, with 94% of the signal matched by the model. This is an exceptional level of fit for this type of modeling; due to space limitations, the waveform comparisons are not shown. The average rake of each subfault is indicated by vectors in Figs. 1 and 2, the vector lengths are proportional to the subfault moment or the inferred subfault slip. The total moment estimate is 4.0×10^{22} N m ($M_w = 9.0$) and the centroid time of the moment rate function is 73.4 s. These values are both consistent with the W-phase moment estimate of 3.9×10^{22} N m and centroid time of 71 s (Ammon *et al.*, 2011). This agreement with very long-period constraints is likely fortuitous, as the P-waves are band-limited by depth-phase interference, but the waveforms are smooth and well-fit, and the signals are not dominated by very short-periods as is the case for most other events, so some constraint on periods out to ∼80–120 s is provided by the P-wave data. Very little smoothing of the subfault moment distribution was used in the inversion; the data are intrinsically fit by smooth solutions. The moment rate function increases rather steadily for about 80 s, then decreases to low amplitude by about 150 s. This is very similar to the source time function Ammon *et al.* (2011) infer from joint inversion of P-waves, Rayleigh wave relative source time functions, and continuous GPS ground motion recordings.

The mapping from subfault seismic moment to subfault slip is shown in Fig. 2, and strongly reflects the fact that the shallower subfaults are located in lower velocity material. This phenomenon is well known, of course, but is particularly dramatic when the rupture extends over a wide fault with variable velocity structure. Slip models from subfault moment distributions in a half-space vary linearly with the subfault moment distributions (Ammon *et al.*, 2011), and it is important to keep in mind the dependence on rigidity structure used when comparing 'derived' slip distributions from seismic models. Geodetic and tsunami modeling inversions are directly parameterized for slip on the fault, as the important material property control on the surface displacements for an elastic half-space is the less-variable Poisson ratio (Okada, 1985), thus comparisons with seismic estimates of slip again must account for the rigidity mapping of the latter. Some studies take the seismic moment distribution obtained for one elastic structure and simply map slip from it using a different elastic structure, but this is not self-consistent; the moment distribution obtained from seismic waves is dependent on the velocity structure used. The effect is not strong for Rayleigh waves, but is significant for Love waves and body waves (e.g., Ferreira and Woodhouse, 2006). While our 1-D source velocity model is an approximation, the slip model is consistent with the seismic moment estimates for that model. We note that one could directly invert P waves for slip by multiplying the Green functions by depth-varying rigidity, with corresponding difference in the intrinsic weighting of the redefined model parameters and with solution smoothing effects acting directly on potency rather than seismic moment estimation. However, with little need for smoothing this is just a linear trade-off in the P wave inversion and no particular advantage is offered by such a reformulation of the problem in this case.

The largest slip in P-MOD2 is concentrated near the trench, and occupies the concave seaward bend in the trench. The bathymetry in this region shows a mild arch, which may reflect topography on the underthrusting plate or plastic deformation of the wedge. A peak slip value of $\sim$63 m is obtained, but little emphasis should be placed on peak values in finite-fault models as they are influenced by the grid discretization, solution smoothing, and the layering of the rigidity structure. The averaged along-dip velocity structures do vary rapidly near the deformed zone in the wedge toe in seismic reflection profiles (Takahashi *et al.*, 2004; Miura *et al.*, 2005), so shallow peaking of the slip is expected for a uniform seismic moment distribution, but the precise slip values are uncertain due to the uncertainties in the velocity model. The average slip over the entire fault model is 15.9 m. Perhaps more meaningful is the average slip over well-resolved regions of the fault. Restricting the averaging to only regions for which the subfault moment is 20 percent of the largest subfault moment, we find an average slip of 20.9 m over 54,400 km^2, with a cumulative seismic moment of 3.8×10^{22} N m.

While the resolution of rake on the fault tends to be limited for a P-wave only inversion, the model exhibits a systematic pattern of slip vector convergence toward the area of major up-dip slip, which is itself perpendicular to the strike. This may be real, given that geodetic displacements on the mainland also have convergence toward this part of the source. One possibility is that this reflects an arching of the interplate zone, although there is no direct resolution of this feature, only the suggestion of it in the bathymetric relief. The seismic moment distribution in Fig. 2 includes some down-dip extension; note that this feature is less evident in the slip calculations due to the increase in rigidity at depth. Short-period P-wave back-projections indicate initial down-dip migration of the short-period energy source, which likely corresponds to this deep seismic moment concentration (Koper *et al.*, 2011). Clearly the up-dip region did not have strong short-period seismic wave radiation despite having very large slip, as no energy is imaged there in the back-projections. This is consistent with the frequency-dependent pattern noted by Koper *et al.* (2011).

Many finite-fault inversions use multiple data types to constrain the rupture, so one can question the use of only teleseismic P waves, even for preliminary results. To check the long-period stability of the results, P-MOD2 displacements were used to compute static motions on Honshu for comparison with the first 15-minute solution for static offset at the ARIA (JPL-GSI) continuous GPS stations. Horizontal and vertical ground motion observations and predictions using Okada (1985) solutions are shown in Fig. 3. The agreement is excellent, indicating, at the least, that the geodetic motions cannot rule out slip extending to the trench. The match is actually better than found for the earlier P-MOD solution which does not reach to the trench, but this may be primarily the result of not allowing the grid to extend quite as far down-dip toward the coast. Using the same P-MOD grid and moving the hypocenter up- or down-dip has secondary effects on the solution; it is mainly allowing the rupture to reach the trench in the first 50 s or so of low rupture velocity expansion that allows seismic moment to be large enough in the shallowest crustal layer to map into very large slip estimates there. The kinematic constraints do strongly influence this solution.

3. Discussion and Conclusions

Significant fault displacement near the trench is a realistic possibility for the great 11 March 2011 Tohoku Earthquake. The precise estimate of slip is highly uncertain, as it depends upon the estimated velocity structure and the general instability of seismic moment determinations for very shallow dip-slip events. However, the general pattern in P-MOD2 is compatible with experiments on varying the source location to match remote DART tsunami observations in the western Pacific (Lay *et al.*, 2011b), and can be reconciled with long-period source inversions that have better intrinsic spatial resolution of seismic moment distribution given that rigidity variations are neglected in some of those models. P-MOD2 is compatible in slip strength and location with an online model produced by Guangfu Shao, Xiangyu Li, and Chen Ji (http://www.geol.ucsb.edu/faculty/ji/), which inverted broadband P-waves, SH-waves, and long-period waves, so there is a suite of seismic evidence for strong up-dip slip all the way to the trench for this event. In addition, direct measurement of seafloor deformation near the toe of the wedge indicates 50 m of ESE displacement close to the trench (JAMSTEC press release: http://www.jamstec.go.jp/j/about/press_release/20110428/reported after the initial submission of this paper). This is very consistent with our final slip model.

One of the important consequences of large slip at shallow depth is the induced change in stresses acting on different fault geometries in the upper and lower plates and along strike of the megathrust. We estimate the stress perturbations for P-MOD2 using Coulomb 3, software produced by S. Toda, R. Stein, J. Lin and V. Sevilgen. Our implementation assumes a half-space with a finite fault having subfault geometries and slip given by the model shown in

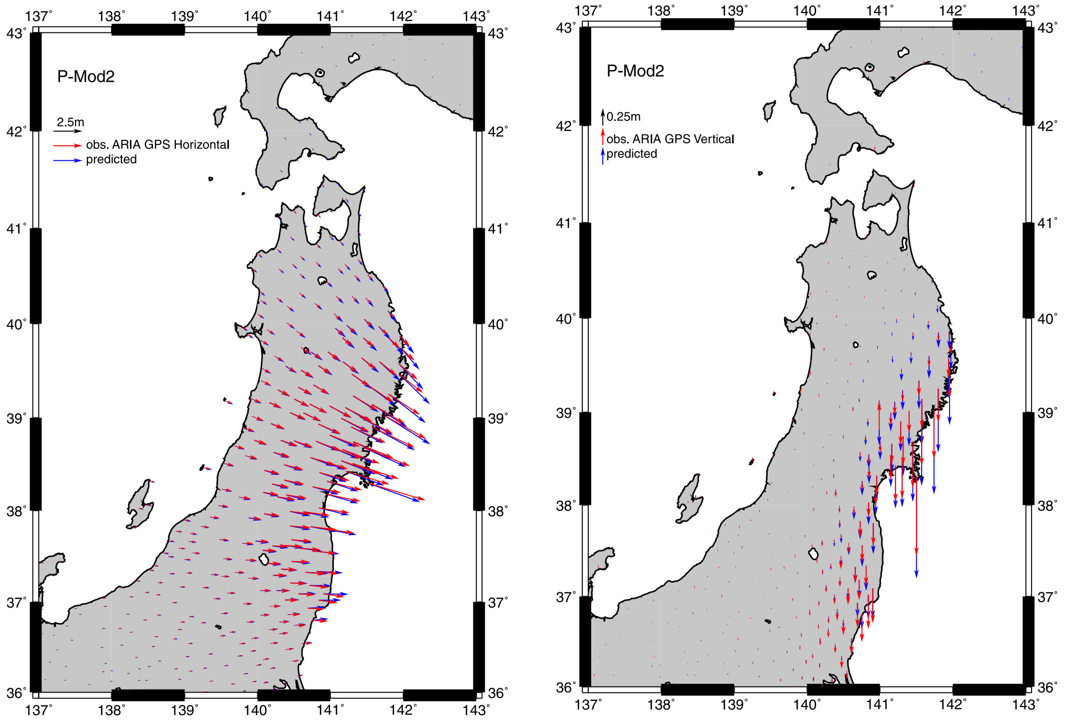

Fig. 3. Maps showing the observed (red vectors) and predicted (blue vectors) static ground motions from continuous GPS stations of project ARIA on Honshu for the 11 March 2011 Tohoku Earthquake and model P-MOD2 in Fig. 1, computed using the half-space solutions of Okada (1985). The horizontal observations (left panel) are very well matched, and most of the much smaller vertical motions (right panel) are well predicted with exception of a few positions near the Honshu coast.

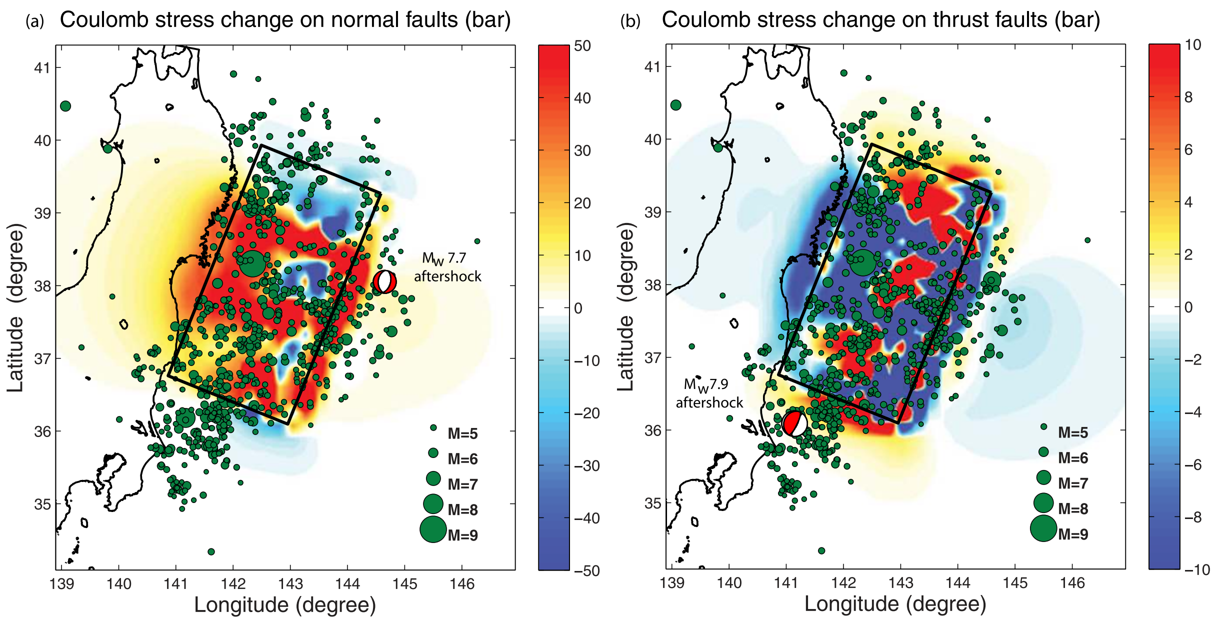

Fig. 4. Maps of the Coulomb stress change predicted for model P-MOD2 in Fig. 1. The grid of the fault model is indicated by the rectangle. Two weeks of aftershock locations from the U.S. Geological Survey are superimposed, with symbol sizes scaled relative to seismic magnitude. The known faulting mechanisms are shown in Fig. 1. (a) The Coulomb stress change averaged over depths of 10–15 km for normal faults with the same westward dipping fault plane geometry as the M_w 7.7 outer rise aftershock, for which the GCMT mechanism is shown. (b) Similar stress changes for thrust faults with the same geometry as the mainshock, along with the M_w 7.9 thrusting aftershock to the south, for which the GCMT solution is shown.

Fig. 2. The half-space solution only has material property sensitivity to Poisson ratio, which is roughly constant in our source structure, so using the seismic slip model estimated in a layered structure to compute static deformations in a homogeneous half-space is reasonable to first order. More detailed calculations with 3D viscoelastic, spherical structures can be pursued, but are unlikely to change the basic comparison here. We have found that use of spherical PREM structure to compute the static displacements had very minor differences from the Okada half-space solutions shown here. We calculate average stress changes over depths of 10–15 km for two fault geometries; a normal

faulting geometry given by the westward dipping plane of the large M_w 7.7 aftershock (Fig. 4(a)) located in the outer rise (strike 182°, dip 42°, rake −100°; Global Centroid Moment Tensor (GCMT)) and a thrust fault geometry similar to the mainshock (strike 202°, dip 12°, rake 90°). A conventional friction coefficient of 0.4 is assumed, but there is little change for values as high as 0.8. Stress changes favoring normal faulting are about 5 bar in the outer rise region where the M_w 7.7 event occurred, but can be several tens of bars in the trench slope region and upper plate region above the megathrust, which has normal faulting aftershocks near the main slip zone (Fig. 1). Stress changes of several bars favoring thrust faulting are produced along strike of the megathrust, including where the largest aftershock, an M_w 7.9 event, occurred (Fig. 4(b)). The distribution of other GCMT focal mechanisms in Fig. 1 show some correspondence with the predicted Coulomb stress variations, but many different fault geometries and depths would need to be evaluated. These calculations can be compared with those for the joint seismic and geodetic inversion model of Ammon *et al.* (2011), which are presented in Lay *et al.* (2011c).

Assuming the general slip distribution shown in Fig. 1 holds up over time, it appears that there is little likelihood of a near-future tsunami earthquake up-dip of the 2011 rupture in the region of the upper plate protuberance into the trench. However, the large slip has contributed to larger than typical Coulomb stress perturbations on outer rise faults and along-strike portions of the megathrust, so it would not be surprising for additional earthquakes to occur in these regions if they have built up strains to near the failure level. If offshore pressure sensors and/or strain records can be related to the co-seismic ocean bottom deformations, additional tests could be made on the slip distribution in the toe of the wedge.

Acknowledgments. This work made use of GMT, SAC and Coulomb 3 software. The IRIS DMS data center was used to access the FDSN seismic data. This work was supported by NSF grant EAR0635570 and USGS Award Number 05HQGR0174. We thank the editor and two anonymous reviewers for their constructive reviews of the manuscript.

References

Ammon, C. J., H. Kanamori, T. Lay, and A. A. Velasco, The 17 July 2006 Java tsunami earthquake, *Geophys. Res. Lett.*, **233**, L234308, doi:10.10239/2006GL028005, 2006.

Ammon, C. J., H. Kanamori, and T. Lay, A great earthquake doublet and seismic stress transfer cycle in the central Kuril islands, *Nature*, **451**, 561–566, 2008.

Ammon, C. J., T. Lay, H. Kanamori, and M. Cleveland, A rupture model of the 2011 off the Pacific coast of Tohoku Earthquake, *Earth Planets Space*, **63**, this issue, 693–696, 2011.

Bilek, S. L. and T. Lay, Tsunami earthquakes possibly widespread manifestations of frictional conditional stability, *Geophys. Res. Lett.*, **29**(14), doi:10.1029/2002GL015215, 2002.

Ferreira, A. M. G. and J. H. Woodhouse, Source, path and receiver effects on seismic surface waves, *Geophys. J. Int.*, doi:10.1111/j.1365-246X.2006.03092.x, 2006.

Fukao, Y., Tsunami earthquakes and subduction processes near deep-sea trenches, *J. Geophys. Res.*, **84**, 2303–2314, 1979.

Hartzell, S. H. and T. H. Heaton, Inversion of strong ground motion and teleseismic waveform data for the fault rupture history of the 1979 Imperial Valley, California, earthquake, *Bull. Seismol. Soc. Am.*, **73**, 1553–1583, 1983.

Ide, S., A. Baltay, and G. Beroza, Shallow dynamic overshoot and energetic deep rupture in the 2011 M_w 9.0 Tohoku-oki earthquake, *Science*, doi:10.1126/science.1207020, 2011.

Kanamori, H., Seismological evidence for a lithospheric normal faulting; the Sanriku earthquake of 1933, *Phys. Earth Planet. Inter.*, **4**, 289–300, 1971.

Kanamori, H., Mechanism of tsunami earthquakes, *Phys. Earth Planet. Inter.*, **6**, 346–359, 1972.

Kanamori, H. and M. Kikuchi, The 1992 Nicaragua earthquake: A slow tsunami earthquake associated with subducted sediments, *Nature*, **361**, 714–716, 1993.

Kanamori, H., L. Rivera, and W. H. K. Lee, Historical seismograms for unraveling a mysterious earthquake: The 1907 Sumatra earthquake, *Geophys. J. Int.*, **183**, 358–374, doi:10.1111/j.1365-246X.2010.04731.x, 2010.

Koper, K. D., A. R. Hutko, T. Lay, C. J. Ammon, and H. Kanamori, Frequency-dependent rupture process of the 2011 M_w 9.0 Tohoku Earthquake: Comparison of short-period *P* wave backprojection images and broadband seismic rupture models, *Earth Planets Space*, **63**, this issue, 599–602, 2011.

Lay, T., C. J. Ammon, H. Kanamori, Y. Yamazaki, K. F. Cheung, and A. R. Hutko, The 25 October 2010 Mentawai tsunami earthquake (M_w 7.8) and the tsunami hazard presented by shallow megathrust ruptures, *Geophys. Res. Lett.*, **38**, L06302, doi:10.1029/2010GL046552, 2011a.

Lay, T., Y. Yamazaki, C. J. Ammon, K. F. Cheung, and H. Kanamori, The 2011 M_w 9.0 off the Pacific coast of Tohoku Earthquake: Comparison of deep-water tsunami signals with finite-fault rupture model predictions, *Earth Planets Space*, **63**, this issue, 797–801, 2011b.

Lay, T., C. J. Ammon, H. Kanamori, M. J. Kim, and L. Xue, Outer trench-slope faulting and the 2011 M_w 9.0 off the Pacific coast of Tohoku Earthquake, *Earth Planets Space*, **63**, this issue, 713–718, 2011c.

Miura, S., N. Takahasi, A. Nakanishi, T. Tsuru, S. Kodaira, and Y. Kaneda, Structural characteristics off Miyagi forearc region, the Japan Trench seismogenic zone, deduced from wide-angle reflection and refraction study, *Tectonophysics*, **407**, 165–188, 2005.

Okada, Y., Surface deformation due to shear and tensile faults in a half space, *Bull. Seismol. Soc. Am.*, **75**(4), 1135–1154, 1985.

Pelayo, A. M. and D. A. Wiens, Tsunami earthquakes: Slow thrust-faulting events in the accretionary wedge, *J. Geophys. Res.*, **97**, 15,321–15,337, 1992.

Polet, J. and H. Kanamori, Shallow subduction zone earthquakes and their tsunamigenic potential, *Geophys. J. Int.*, **142**, 684–702, 2000.

Simons, M. *et al.*, The 2011 Magnitude 9.0 Tohoku-Oki earthquake: Mosaicking the megathrust from seconds to centuries, *Science*, **332**, doi:10.1126/science.1206731, 2011.

Takahashi, N., S. Kodaira, T. Tsuru, J.-O. Park, Y. Kaneda, K. Suyehiro, H. Kinoshita, S. Abe, M. Nishino, and R. Hino, Seismic structure and seismogenesis off Sanriku region, northeastern Japan, *Geophys. J. Int.*, **159**, 129–145, 2004.

T. Lay (e-mail: tlay@ucsc.edu), C. J. Ammon, H. Kanamori, L. Xue, and M. J. Kim